Separation Science and Technology
Publication details, including instructions for authors and subscription information:
http://www.informaworld.com/smpp/title~content=t713708471

Liquid Chromatography in Helically Coiled Open Tubular Columns

R. Tijssen[a]
[a] KONINKLIJKE/SHELL-LABORATORIUM SHELL RESEARCH B.V. AMSTERDAM, THE NETHERLANDS

To cite this Article Tijssen, R.(1978) 'Liquid Chromatography in Helically Coiled Open Tubular Columns', Separation Science and Technology, 13: 8, 681 — 722
To link to this Article: DOI: 10.1080/01496397808057121
URL: http://dx.doi.org/10.1080/01496397808057121

SEPARATION SCIENCE AND TECHNOLOGY, 13(8), pp. 681–722, 1978

Liquid Chromatography in Helically Coiled Open Tubular Columns

R. TIJSSEN

KONINKLIJKE/SHELL-LABORATORIUM
SHELL RESEARCH B.V.
AMSTERDAM, THE NETHERLANDS

Abstract

Limitations on pressure, packing procedures, and extra-column broadening make it unlikely that the use of particles smaller than 2 μm in packed columns for liquid chromatography will be effective. We have therefore investigated the potential of alternative column types, in particular open tubular columns, for LC. When tubes are tightly coiled into helices, the radial mass transfer in the mobile phase is greatly enhanced by radial convection, called secondary flow, originating from centrifugal forces.

A criterion is developed for the velocity up to which the classical description of axial dispersion in straight columns, after Golay, can be expected to hold. A correction for curvature effects is given for intermediate and high velocities. In principle, the corrected equations enable one to determine molecular diffusion constants from peak broadening within short times, even for macromolecular solutions. At high velocities a drastic decrease in peak broadening is expected, and this was experimentally confirmed for nonretained solutes. The separation speed increases at least quadratically with velocity such that 10^3 to 10^4 plates/sec can easily be obtained at pressures not higher than those presently needed for packed columns. The coating of a stable homogeneous layer of stationary phase onto the column wall has been only partially solved. Experience gained with various types of coating is discussed.

INTRODUCTION

Resolution in column chromatography is greatly influenced by the choice of operating parameters such as the particle size of the packing material and the velocity of the mobile phase. How much can be achieved

by the systematic application of ever smaller particles alone is illustrated by the development of LC into the modern high-performance LC (HPLC), which is comparable to GC with regard to efficiency and analysis time (*1*). Whether this trend to particles even smaller than the now common size of 2 to 5 μm has any future depends largely on the increasingly difficult problems that accompany the packing of such small particles randomly into a column. Particles of 2 to 5 μm can still be packed by the well-known slurry methods, but the gain in efficiency is less than that predicted by the theoretical relation (*2*) $H \doteqdot d_p^2$. In practice, plate height is far less dependent on particle size because of the ever-increasing mutual interaction between smaller particles. As packing procedures that avoid this effect are unknown and difficult to develop, there is little hope that particles smaller than, say, 1 μm will ever be packed effectively.

Therefore, it seems worthwhile to look for alternative column types which are in principle capable of generating higher plate numbers and/or higher separation speeds than the presently available ones, i.e., 5×10^4 plates and 100 plates/sec typically for well-packed columns. More specifically one may ask whether open tubular columns, which have been used successfully in GC, can also be applied in LC. Up to now the slow radial mass transport in the mobile phase has prevented the use of these columns in LC, apart from preliminary reports by Jentzsch et al. (*3*), Horvath et al. (*4*), and Nota et al. (*5*). Normally this transport is governed by molecular diffusion alone and in gases where the diffusion coefficient, D_m, ranges from 10^{-2} to 10^{-1} cm^2/sec, radial diffusion is sufficiently fast to result in very efficient capillary columns in GC. In liquids, where D_m is some 5 orders of magnitude smaller than in gases, viz., 10^{-5} to 10^{-7} cm^2/sec, the resulting rate of mass transport is far too low to yield acceptable plate heights.

After Golay (*6*), the plate height, H, for straight open columns can be described by

$$H = \frac{2D_m}{\bar{u}} + \frac{2\kappa_0 R_c^2}{D_m}(f(k))_0\bar{u} + C_s\bar{u} \tag{1a}$$

or

$$H = \frac{B}{\bar{u}} + C_m\bar{u} + C_s\bar{u} \tag{1b}$$

where B represents axial molecular diffusion, C_m is the combined action of broadening by the velocity profile and counteracting radial diffusion in the mobile phase, and C_s describes the contribution of the stationary phase.

κ is called the velocity profile factor which, for straight columns, is a constant, $\kappa_0 = 1/48$, determined by the parabolic velocity profile. $f(k)$ represents the influence of the assumed partition equilibrium of the solute molecules between the mobile and the stationary phase, and is called the retention function. It is seen that C_m becomes large for the small diffusion constants of liquids.

However, from Eq. (1) we observe that, apart from C_s, the axial dispersion of a solute zone can be represented by a summation of contributions from diffusion and convection mechanisms, i.e., B and C_m. By analogy, we assume that the radial dispersion can also be represented by a combination of molecular diffusion and convection. Thus, after the introduction of a suitable radial convection, diffusion can be aided, resulting in a stimulated radial dispersion coefficient, D_r. In earlier work (*7*, *8*) we showed how this can be done by using tightly coiled helical tubes. Then centrifugal forces generate the so-called secondary flow in radial directions, resulting in an assumed radial dispersion coefficient, D_r, given by

$$D_r = D_m + D_s \tag{2}$$

Equation (2) is formally equivalent to the coupling concept of Giddings (*2*) and the widely used description of so-called eddy diffusion in packed bed systems, both expressing the addition of diffusion and convection processes.

A first rough estimate (*7*) indicated that this enhanced radial dispersion easily surpasses molecular diffusion alone, especially for liquids at sufficiently high velocities. In this paper a better estimate of the radial mass exchange will be presented, together with an improved description of the influence of changes in velocities without the need for an explicit knowledge of the accompanying velocity profiles.

The potential of open-tube liquid chromatography in terms of separation speed will be discussed as well as its use for the rapid determination of diffusion constants. It will be shown that, in contrast with packed columns, open tubular columns in a helical configuration (HOT columns) show great promise with regard to zone dispersion. The separation speed increases at least quadratically with velocity and is nearly always superior to that of packed columns, at high velocities even by several orders of magnitude. Hence the optimization of HOT columns is a very desirable future goal, whereas short-term optimization of packed columns for LC can probably be achieved only by improving selectivity instead of dispersion.

In sum, the prospects of using HOT columns seem to disagree with

Horvath's view (*4*) that only packed columns should be used in LC. The recent statement by Halász (*9*) that the use of open columns in LC will have to wait another decade also seems to be contradicted.

THEORETICAL

A description of peak dispersion in HOT columns (and many other column types) can in principle be obtained from the solution for the concentration in the mass balance equations. The relatively simple geometry of open tubes permits analytical solutions, such as those of Taylor (*10*), Aris (*11*), and Golay (*6*), rather than the use of semiempirical correlations as is common in the technology of packed-bed systems. Analytical solutions are to be preferred as they allow interpretations with a physical meaning. For HOT columns these solutions can be obtained while simplifying the mathematical problem by the assumption earlier discussed that radial mass transport can be characterized by an overall transport number, D_r (Eq. 2). This can be proved (*8*) to be permissible as an average over the cross section of the column and the only assumption thus left is that the same transport number, D_r, applies to every local volume element.

The next section is devoted to a physical model for the contribution of secondary flow (D_s) to D_r. This model differs from our earlier viewpoint (*7*, *8*) that the convective contribution as such causes radial mixing and is based on the interaction of molecular diffusion with radial flow patterns.

Radial Dispersion in Helices

The phenomenon of secondary flow has been described well at low velocities by Dean (*12*) and Topakoglu (*13*) and at high velocities by Adler (*14*), Ito (*15*), and Mori and Nakayama (*16*). Several numerical calculations were recently published (*17–21*). The characteristic radial circulation patterns of secondary flow are shown schematically in Fig. 1 together with the accompanying axial velocity profiles. It can be seen that at intermediate velocities the secondary flow tends to divide the main flow into two equal halves. This effect can easily be verified by dye tracer experiments in transparent coils. In a first rough approximation the column can be looked upon as consisting of two equal parallel columns, each having a center line determined by the circulation centers (see Fig. 1) and thus an approximate radius of $\frac{1}{2}R_c$. Thus diffusion distances are decreased by a factor of about 2, which results in a C_m-term contribution to the plate height that is smaller by a factor of about 4.

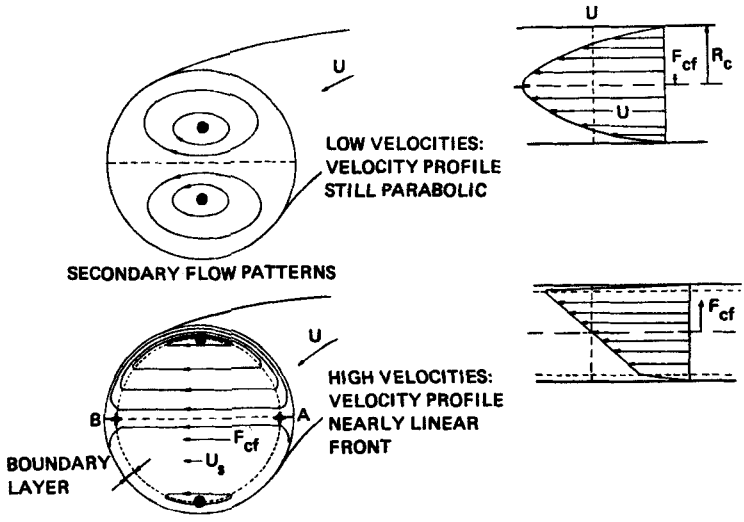

FIG. 1. Schematic representation of radial secondary flow patterns and axial velocity profiles at low (upper figures) and high (lower figures) velocities. Circulation centers are depicted by dots.

The centers of circulation within each of the parallel "columns" are located near each midpoint at lower velocities but tend to approach the column wall with increasing velocity. Thus at high velocities a boundary layer flow occurs, which can also be visualized by dye tracer experiments. Now mass exchange by diffusion is rapid because of the very short distances between all layers with different velocities in the thin boundary layer. As the flow is circulating rapidly, the fluid leaving the boundary layer enters the core of the flow at all points along the column wall. In this way mass exchange within the boundary layer leads to mass exchange throughout the whole cross section. Hence, in general, radial mass exchange is dominated by the region with the highest radial streamline density and the exchange time, τ_m, associated with that region. Clearly, at high velocities the boundary layer dominates and, as D_m will be negligible compared with D_s, $D_r \cong D_s$ (from Eq. 2) can be calculated straightforwardly from the general relation (*1*, *2*) between average squared displacement $\overline{d^2}$, diffusion or dispersion coefficient D, and appropriate time τ during which the dispersion mechanism is acting:

$$D_r \cong D_s = \frac{\overline{d^2}}{2\tau_m} \tag{3}$$

Reasonable assumptions for the extent δ of the boundary layer can be made (*7*, *14*, *16*, *22*), and upon equating $\overline{d^2}$ and δ^2 only mixing time τ_m is to be determined in order to find D_r from Eq. (3).

One has to realize that τ_m is not merely determined by diffusion because the effect of the curvature of the boundary layer itself has to be included. This effect is important as the boundary layer is a sharply curved flow channel (the radius of curvature approximately equals the column radius, R_c) in which appreciable velocities can occur. Thus, again, centrifugal forces are active, resulting in an extra contribution of secondary flow to exchange within the boundary layer. Taking this into account, we can express D_s in terms of secondary flow velocity, u_s, and boundary layer thickness δ, a result which is discussed further in the section entitled "Results and Discussion."

In calculating D_s for intermediate velocities, we observe from Fig. 1 that wall and core regions are of comparable size now, as the center of circulation is more or less central in each half of the column cross section. This implies that exchange in neither of the regions is dominating. Assuming that the contributions of both regions can be added, and taking into account the time fractions spent in both regions (t_w/t_0 and t_c/t_0, respectively, where $t_0 = t_w + t_c$), we have

$$D_s = \frac{t_w}{t_0} D_w + \frac{t_c}{t_0} D_c \tag{4}$$

After division of the cross section into wall and core regions (*22*), estimates of the time fractions can be made, whereas both D_w and D_c follow from Eq. (3) applied to the respective regions. Again, the resulting

TABLE 1

Theoretical Relations for Radial Dispersion in Helical Open Tubular Columns

No.	Equation		Conditions
I	$\frac{D_r}{D_m} = 1 + \frac{De^2Sc}{270}$	(5)	$De^2Sc < 2300$; low velocities in gases; very low velocities in liquids
II	$\frac{D_r}{D_m} = 6.39$	(6)	$De^2Sc > 2300$
III	$\frac{D_r}{D_m} = \frac{De^{3/2}Sc^2}{3.4 \times 10^4}$	(7)	$De > 100$; $Sc < 4$; high velocities in gases
IV	$\frac{D_r}{D_m} = \frac{De^{3/2}Sc}{8 \times 10^3}$	(8)	$De > 100$; $Sc > 4$; high velocities in liquids

expression for D_s is given in terms of u_s. Use of the experimental relation, Eq. (49), describing u_s as a function of the flow velocity, permits the elimination of u_s from the expressions for D_s. The resulting expressions are summarized in Table 1, where the Dean number, De, is a dimensionless velocity (Reynolds number, Re) corrected for curvature by a factor $\lambda^{1/2}$, the square root of the so-called aspect ratio (= column radius/radius of curvature).

Velocity Profiles and Axial Dispersion

In the absence of a stationary phase the formal mass balance to be solved reads in polar coordinates (*23*)

$$\frac{\partial c}{\partial t} = D_m \nabla^2 c - \left(u_z \frac{\partial c}{\partial z} + u_r \frac{\partial c}{\partial r} + \frac{u_\varphi}{r} \frac{\partial c}{\partial \varphi} \right) \tag{9}$$

For simplicity a cylindrical rather than a toroidal coordinate system is chosen. Even when all velocity components are known (*12–16*), this balance can only be solved by numerical techniques, as recently discussed by Janssen (*24*, *25*). However, if the action of radial convection terms in u_r and u_φ is replaced by the equivalent action of radial dispersion with coefficient D_r, developed in the previous section, we have instead of Eq. (9)

$$\frac{\partial c}{\partial t} = D_m \frac{\partial^2 c}{\partial z^2} - u_z \frac{\partial c}{\partial z} + D_r \nabla_{r,\varphi}{}^2 c \tag{10}$$

This equation can be solved analytically along the lines discussed previously (*8*). Recently, Wong et al. (*26*) used analogous reasoning to express secondary flow convection by an effective dispersion term, in their case even directly in terms of axial dispersion.

The resulting expression for plate height to be derived from Eq. (10) is analogous to the Golay equation (Eq. 1), with the advantage that now for every velocity profile κ as well as the retention function $f(k)$ and D_r are known (*8*):

$$H = \frac{2D_m}{\bar{u}} + \frac{2\kappa R_c{}^2}{D_r} f(k)\bar{u} + C_s\bar{u} \tag{11}$$

Although many descriptions of velocity profiles are known (*12–16*), they are reliable only at rather low velocities or at impractical high velocities. At low velocities a complication arises as neither the profile by Dean (*12*) nor that by Topakoglu (*13*) (which differs from the former by containing more terms in a series) can be transformed into the power series

(*8*) required for calculating κ. Thus, especially in the low and intermediate velocity regions, we need alternative methods for calculating the velocity profile factor.

We investigated the possibility of using the Topakoglu profile in a perturbation method earlier applied in heat-transfer problems (*27*), and obtained (*22*)

$$\kappa = \frac{1}{48} j^2 \qquad (\mathrm{De} < 20) \tag{12}$$

j, connected with the friction factor ratio for helical and straight columns under equal flow conditions, is a complex function of velocity

$$j \cong f/f_0 = 1 + \alpha(\mathrm{De}) \tag{13}$$

α(De) follows from experiments and is described by Eq. (58). Realizing that Eq. (12) is restricted to De < 20, i.e., $\alpha(\mathrm{De}) \approx 0$ and $\kappa \approx 1/48$, we looked for a more general alternative method that would yield κ at every required velocity. This could be achieved by expressing κ in terms of the dimensionless mass transport number, Sh (Sherwood number). From the definition of κ (*8*)

$$\kappa = \frac{D_r}{2R_c^2 \bar{u}} \frac{H_m}{f(k)} = -\frac{D_r}{\pi R_c^4 \bar{u}^2} \frac{1}{(\partial c_m/\partial z)} \frac{1}{f(k)} \int_A (c_m - c_m^*) u \, dA \tag{14}$$

it can be derived (*22*) that with infinite retention ($k = \infty$)

$$\kappa = [\mathrm{Sh} f(k = \infty)]^{-1} \tag{15}$$

For the limiting case of very low velocities, κ should obey Golay's result, $\kappa_0 = 1/48$ and $f(k = \infty) = (f(k = \infty))_0 = 11$, so

$$\kappa = (11\mathrm{Sh})^{-1} \tag{16}$$

Equation (16) is only approximative for the higher velocities in non-straight columns as $f(k = \infty)$ is less than 11, to be proved in the following. Often, however, Sh numbers are not known better than within a factor of 2, especially in using correlations. Thus the use of the factor 11 in Eq. (16), strictly valid only for straight tubes, is allowed in view of experimental errors. Although only approximative, this simple relation has the great advantage that, once Sh is known from experiments, κ is known without the need for an explicit knowledge of the velocity profile.

Experimental determinations of transport numbers such as Sh or the analogous Nu (Nusselt) number for heat transfer have been carried out by a number of workers and many velocity profiles depending on column

geometries and velocity (laminar and turbulent) for different types of fluids (gases and liquids, Newtonian and non-Newtonian) were included in these experiments (*27–29*). As much more data on heat transfer in tubes are reported in the literature, we applied the analogy principle (*23*) which states that for the same geometrical conditions Sh replaces Nu for mass instead of heat transfer.

Equation (16) is most easily tested for the case of a straight pipe where $Nu_0 = Sh_0 = 48/11$ both experimentally and theoretically (*22*, *27*). Indeed, $\kappa = \kappa_0 = 1/48$ is then obtained. At intermediate velocities in helices ($De < 20$) we find (*22*)

$$Sh = Sh_0 j^{-2} \qquad (De < 20) \tag{17}$$

in perfect analogy with the experimental and theoretical heat transfer case considered by Özisik and Topakoglu (*27*). At higher De numbers we now use Eq. (16) together with available heat transfer correlations based on experiments or numerical calculations. From the recent work of Kalb and Seader (*28*) and Dravid et al. (*29*) we conclude that a reliable correlation for the Sherwood number is given by

$$Sh = (3/4)De^{1/2}Sc^{0.14} \qquad (De > 50) \tag{18}$$

Combining this with Eq. (16), we have

$$\kappa = (8.25De^{1/2}Sc^{0.14})^{-1} \qquad (De > 50) \tag{19}$$

Apart from uncertainty in the numerical constant 8.25, this relation reflects an important property, viz., a square-root decrease in κ with increasing velocity, i.e., the peak broadening by velocity profiles is less at higher velocities. This is an important correction to our earlier estimate (*7*, *8*) where κ is a constant of about 1/20 based on an assumed constant inclination $(3/5)(\bar{u}/R_c)$ of the front of the velocity profile:

$$\frac{u_z}{\bar{u}} = \frac{6}{5}(1 - \rho^{10}) + \frac{3}{5}\rho \cos \varphi; \qquad \rho = r/R_c \tag{20}$$

Here the 10th power function is an assumed correction for the boundary layer region where the local velocity, u_z, should drop to zero at the column wall. The inclination of 3/5 in Eq. (20) is in close agreement with the average experimental value often reported in the literature (*22*), having a value of 2/3 in the high-velocity region ($200 < De < 600$). Introducing a slight correction to the Mori profile, to the effect that the inclination of the front at high velocities becomes 2/3, and using the same 10th power

correction as in Eq. (20), we have

$$\frac{u_z}{\bar{u}} = g_1\frac{6}{5}(1 - \rho^{10}) + g_1 g_2\frac{2}{3}\rho\cos\varphi \tag{21}$$

with

$$g_1 = \left[1 - \frac{3.09}{\mathrm{De}^{1/2}} + \frac{4.08}{\mathrm{De}}\right]^{-1}; \qquad g_2 = \left[1 - \frac{3.09}{\mathrm{De}^{1/2}} + \frac{0.51}{\mathrm{De}}\right]$$

Equation (21) can be regarded as the best available analytical expression for the velocity profile in coiled tubes at high velocities; g_1 and g_2 are correction factors which reflect the velocity dependence of boundary layer thickness, δ, which after Mori (*16*) reads

$$\frac{\delta}{R_c} = \frac{4.631}{\mathrm{De}^{1/2}} - \frac{0.766}{\mathrm{De}} \qquad (\mathrm{De} > 50) \tag{22}$$

An important improvement of Eq. (21) vis-à-vis Eq. (20) is that the inclination of the front of the velocity profile is a function of velocity ($\frac{2}{3}g_1g_2$) instead of a constant. Thus κ should indeed be a function of velocity in accordance with the prediction by Eq. (19). Equation (21) is also important for the calculation of the retention function, $f(k)$ (*8*), which does not follow from the Sh-correlation approach leading to Eq. (19), as this is based on the limiting situation $k = \infty$. The only possible way to obtain $f(k)$ is to perform the integral in Eq. (14), applying the best available expression for velocity, Eq. (21). Along the lines of earlier work (*8*) we obtain (*22*)

$$f(k)\kappa = g_1\left[\frac{7}{24} - \frac{1}{28(1+k)}\right] - g_1^2\left(\frac{1}{7.814} - \frac{g_2}{30.857}\right) - \frac{1+2k}{8(1+k)^2} \tag{23}$$

In the high-velocity limit $\mathrm{De} \to \infty$, $f(k)$ is then found as

$$f(k)\kappa \cong \frac{1 + 3k + 5.5k^2}{28(1+k)^2} \tag{24}$$

which is very similar to an earlier expression (*8*) derived from Eq. (20) with $\kappa \approx 1/20$:

$$f(k) \cong \frac{1 + 3k + 6k^2}{(1+k)^2} \tag{25}$$

Because Eq. (25) deviates very little from Eq. (24), we go on using it in the

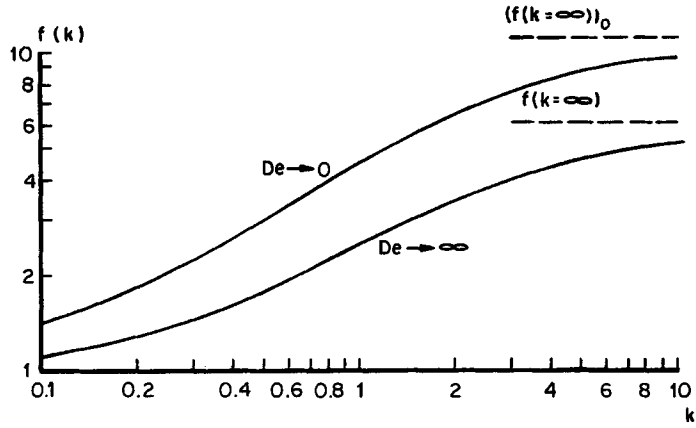

FIG. 2. Retention function for the C_m-term caused by partition equilibrium. $[f(k)]_0$ after classical Golay equation. $f(k)$ predicted for HOT columns at high velocities.

following for simplicity in the calculations. $f(k)$ in Eq. (25) has lower numerical values than $(f(k))_0$, the retention function for the straight column (*6*, *8*, *11*) or the low-velocity region in coiled columns (De < 20):

$$(f(k))_0 = \frac{1 + 6k + 11k^2}{(1 + k)^2} \tag{26}$$

Figure 2 gives a comparison between the limiting forms, Eqs. (25) and (26). At intermediate velocities the retention function $f(k)$ lies somewhere between the functions shown in Fig. 2. Thus, in fact, a constant somewhere in between 11 and 6 should have been used in Eq. (16) instead of the constant 11. This is not done here in view of the uncertainties offered by the Sh correlations and the fact that the constant, representing $f(k = \infty)$, depends on the actual shape of the velocity profile.

Total Axial Dispersion

At this stage it is possible to combine the expressions for velocity profile factors, retention function, and radial dispersion. The results for the different cases in Table 1 are collected in Table 2, where axial dispersion is expressed in terms of Peclet numbers rather than in plate height. This allows the relations to be tested on a dimensionless basis irrespective of column dimensions (R_c and L). The radius-based Peclet number, Pe_r, is

defined as $(H/4R_c)^{-1}$, so for a nonretained solute ($C_s = 0$) and neglecting axial molecular diffusion ($2D_m/\bar{u}$) in Eq. (11), we have

$$\frac{1}{\mathrm{Pe}_r} = \frac{H}{4R_c} = \frac{\kappa}{4}\frac{\mathrm{ReSc}}{(D_r/D_m)} \tag{27}$$

The length-based Peclet number $\mathrm{Pe}_L = (H/2L)^{-1}$ is simply related to Pe_r and plate number:

$$\frac{1}{\mathrm{Pe}_L} = \frac{H}{2L} = \frac{1}{2n_{th}} \tag{28}$$

and with Eq. (27):

$$\frac{1}{\mathrm{Pe}_L} = \frac{2R_c}{L}\frac{1}{\mathrm{Pe}_r} \tag{29}$$

TABLE 2

Theoretical Expressions for Axial Dispersion in Helical Open Columns

No.	Equation		Conditions
I	$\frac{1}{\mathrm{Pe}_r} = \frac{\mathrm{ReSc}}{192\left(1 + \frac{\mathrm{De}^2\mathrm{Sc}}{270}\right)} j^2 f(k)$	(30)	$\mathrm{De}^2\mathrm{Sc} < 2300$
II	$\frac{1}{\mathrm{Pe}_r} = \frac{1}{287}\frac{\mathrm{Re}^{1/2}\mathrm{Sc}^{0.86}}{\lambda^{1/4}} f(k)$	(31)	$\mathrm{De} < 100$ gases
	$\frac{1}{\mathrm{Pe}_r} = \frac{\mathrm{ReSc}}{1227} j^2 f(k)$	(32)	$\mathrm{De} < 100$ liquids
III	$\frac{1}{\mathrm{Pe}_r} = \frac{1035}{\mathrm{ReSc}^{1.14}\lambda} f(k)$	(33a)	$\mathrm{De} > 100$ gases via Sh correlation
	$\frac{1}{\mathrm{Pe}_r} = \frac{305}{\mathrm{Re}^{1/2}\mathrm{Sc}\lambda^{3/4}} f(k)$	(33b)	$\mathrm{De} > 100$ gases via Mori profile
IV	$\frac{1}{\mathrm{Pe}_r} = \frac{242}{\mathrm{ReSc}^{0.14}\lambda} f(k)$	(34a)	$\mathrm{De} > 100$ liquids via Sh correlation
	$\frac{1}{\mathrm{Pe}_r} = \frac{71.4}{\mathrm{Re}^{1/2}\lambda^{3/4}} f(k)$	(34b)	$\mathrm{De} > 100$ liquids via Mori profile

For straight columns, Eq. (27) becomes

$$\frac{1}{(\mathrm{Pe}_r)_0} = \frac{\mathrm{ReSc}}{192} \tag{35}$$

which shows that $v = \mathrm{ReSc}$ can be used as the relevant dimensionless

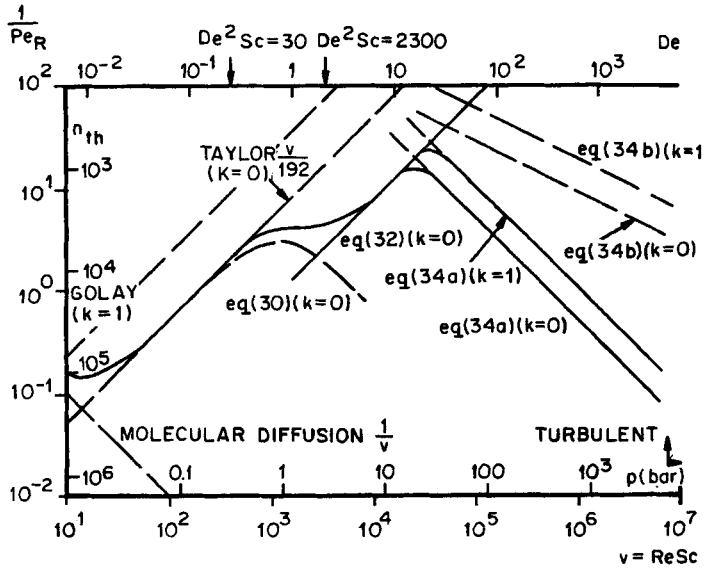

FIG. 3. C_m-term in HOT columns. $\lambda = 1/10$, $k = 0$ and 1, Sc = 500, R_c = 0.0125 cm, and L = 772 cm.

velocity. Figure 3 gives a graphical representation of the dispersion behavior of a normal liquid (Sc = 500) flowing through a tightly coiled tube ($\lambda = 1/10$) with a velocity range extending over 6 decades.

In the nonretained situation ($f(k) = 1$) above the chromatographic optimum velocity ($v \cong 14$), dispersion after Taylor (Eq. 35) is expected first up to velocities corresponding to $De^2Sc \cong 30$ or $v \cong 500$ (see Eq. 30). At velocities $v > 5 \times 10^3$ we expect a constant deviation to occur from Taylor's expression according to Eq. (32). A maximum is expected to appear at velocities $v \cong 10^4$ from combining Eqs. (32) and (34a).

An important descending behavior of $1/Pe_r$ at higher velocities is predicted by both Eq. (34a) (based on κ from the Sh correlation) and Eq. (34b) (based on κ for the corrected Mori velocity profile), but they are seen to disagree in Fig. 3.

PROSPECTS AND LIMITATIONS OF HOT COLUMNS

The possible use of HOT columns in the rapid determination of molecular diffusion constants is discussed in the Appendix; in this section some consequences of their use in chromatography are considered.

Separation Speed and Pressure Drop

HOT columns differ from other types in having the important property that at higher velocities an increasing number of plates are generated within ever shorter residence times (see Fig. 3). This means that the separation speed (i.e., the number of plates per second) increases sharply with velocity. From Eq. (34a) for liquids it follows that

$$n_{th} = \frac{\mathrm{Pe}_L}{2} = \frac{L}{4R_c}\mathrm{Pe}_r = \frac{L}{R_c}\frac{\mathrm{ReSc}^{0.14}\lambda}{968} \tag{36}$$

and

$$\frac{n_{th}}{t} = n_{th}\frac{\bar{u}}{L} = \frac{\mathrm{De}^2\mathrm{Sc}^{0.14}}{1936{R_c}^2}\nu \tag{37}$$

Equation (37) shows that the separation speed increases even quadratically with velocity, whereas in packed LC columns there is only a square-root dependence (*1*). Numerical values are also quite high and in fact seldom below the value for the separation speed of a typical modern HPLC column. Figure 4 clearly demonstrates the great potential of HOT columns for LC with short residence times.

Two practical problems must be considered. First, analysis times become short (of the order of minutes and seconds), and second, a high velocity requires a relatively high pressure. Although the handling times of modern data systems are sufficiently short, the response times of detectors can be a limitation in the practical application of HOT columns. On the other hand, the pressure drop is only moderately higher than that for straight open tubes since the flow is still laminar up to very high velocities (*30*): $\mathrm{Re}_{crit} > 10^4$. In fact, the pressures do not exceed those already in use for packed LC columns, as can be deduced from the experiments on friction factors (see Eqs. 13 and 58). The pressure drop can be found from

$$\Delta p = \frac{4\rho L\nu^2}{{R_c}^3}\mathrm{Re}[1 + \alpha(\mathrm{De})] \tag{38}$$

$\alpha(\mathrm{De})$ is negligible for $\mathrm{De} < 50$, and $\alpha = 1$ for $\mathrm{De} = 400$, i.e., the pressure drop is doubled in comparison with a straight column.

Regarding $\mathrm{De} = 400$ as a practical high-velocity limit, it follows from Eq. (38) that

$$\Delta p \cong \frac{8\rho L\nu^2}{{R_c}^3}\mathrm{Re} \cong 10^{-9}\frac{L}{{R_c}^3}\mathrm{Re} \tag{39}$$

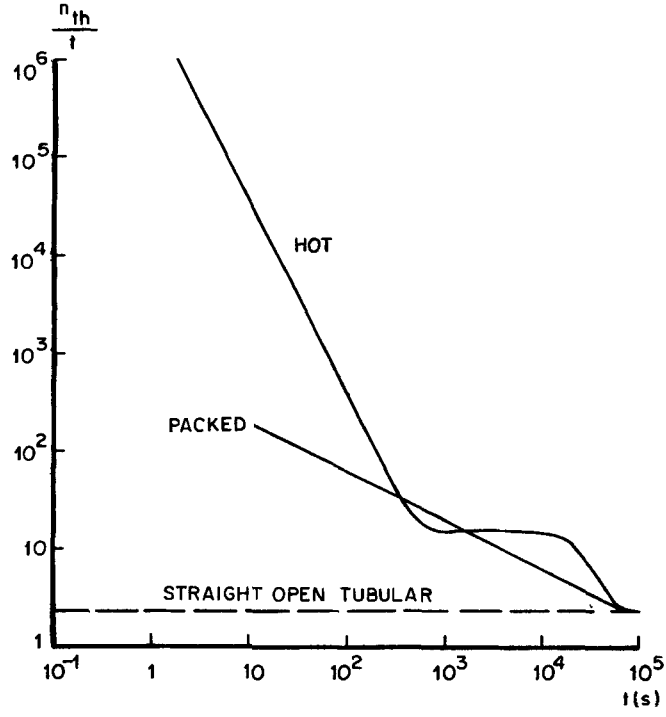

FIG. 4. Comparison between separation speeds of typical HOT and packed LC columns. HOT columns: $L = 10^4$ cm, $R_c = 10^{-2}$ cm, $\lambda = 1/10$, and $(n_{th}/t) = 0.1\mathrm{De}^2 = 4 \times 10^6/t^2$. Packed columns: $L = 10$ cm, $d_p = 5 \times 10^{-4}$ cm, $H = 5. \times 10^{-3} u^{1/2}$, and $(n_{th}/t) = 6 \times 10^2/t^{1/2}$.

(p in bar). For example, in a column with $R_c = 0.0125$ cm and $\lambda = 1/10$, De = 400 (or Re = 1265) is reached at a pressure drop of 500 bar when the column length, L, is 772 cm. This column contains 1.9×10^4 plates generated within 1.5 sec.

Of course the undisturbed detection of, say, 10 to 20 peaks within short residence times of the order of 10 sec offers a real detector problem in view of the common response times of about 1 sec. It seems worthwhile to tackle this problem of developing very rapid detectors in the future, taking into account the great potential offered by HOT columns.

Let us now turn to the limitations introduced by the application of a stationary phase.

Retention and Axial Dispersion

The use of a stationary phase involves at least one more contribution to zone broadening, viz., the C_s term (Eq. 11), which contributes to the plate height with a linear velocity dependence. Another possible contribution arises from so-called interphase and interfacial resistance (*26*, *31*). In the situation where the stationary phase is distributed over the column wall as a perfect flat film with thickness δ_f, irrespective of the form of the velocity profile the C_s term is given by (*8*)

$$C_s = \frac{2}{3}\frac{k}{(1+k)^2}\frac{{\delta_f}^2}{D_m} \tag{40}$$

From $H = C_s\bar{u}$ and Eq. (34a) it is seen that C_s dominates over C_m at velocities corresponding to

$$\mathrm{De}^2\mathrm{Sc} > 608\,\frac{1+3k+6k^2}{k}\left(\frac{R_c}{\delta_f}\right)^2 \tag{41}$$

This sets an upper limit to the velocity that can be applied in practice, as can be seen from the solid lines in Fig. 5, calculated for the case $k = 1$, the value for which C_s is a maximum (see Eq. 40). The more plates required, the greater are the constraints to be met by the layer thickness, δ_f, which is the determining variable of C_s. In order to obtain 10^3 to 10^4 plates, thin films are obviously required, but films of about 1 μm are permissible (see Fig. 5), which is comparable to the situation for capillary columns in GC. For a 1 μm film in a column with radius $R_c = 0.0125$ cm, the phase ratio V_s/V_m, which equals $2\delta_f/R_c$, is 1/62.5. This means that in order to obtain capacity factors $k = K(V_s/V_m)$ of at least 0.1, a practical requirement for separation, the partition coefficients K should be greater than 10. This is not a stiff requirement, but for more favorable thinner films, e.g., $\delta_f = 0.1$ μm, K should be higher than 100, pointing to a typical field of application of HOT columns to strongly interacting or heavy substances.

Although it is still uncertain if the effect of both interphase and interfacial resistances is present or not as a contribution to zone spreading, its advocates (*26*, *31*) state that slowness of mass transfer of these types results in an extra C term, C_i, which can even be the major contribution to the total C term. In straight columns its contribution to the plate height is linear with velocity and so increases with velocity like the C_s contribution from which it is, in fact, distinguishable only because of a different retention function, $f(k)$. Based on discussions in the literature (*23*, *32–34*), it is assumed here that interfacial resistance (in the phase boundary itself) is

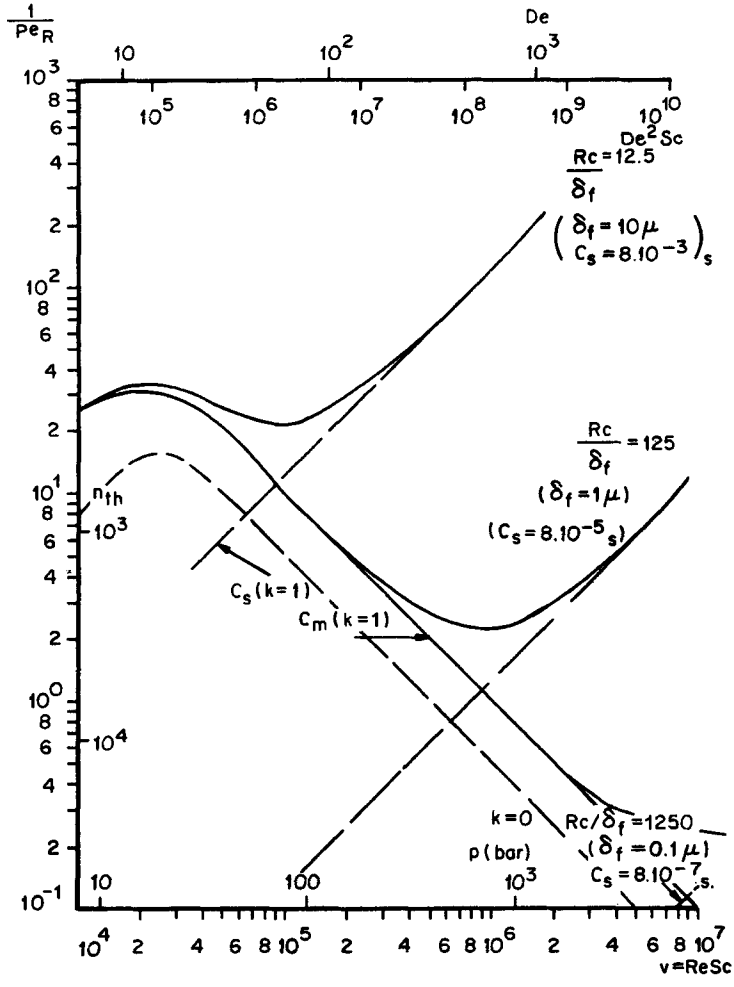

FIG. 5. Limitation of increase in efficiency by C_s-term in HOT columns (R_c = 0.0125 cm, Sc = 500).

absent. For the interphase resistance contribution, expressed in Peclet numbers, C_i reads (*26*)

$$\frac{1}{\mathrm{Pe}_i} = \frac{H_i}{4R_c} = \frac{1}{2}\left(\frac{k}{1+k}\right)^2 \frac{\bar{u}}{k_m} \tag{42}$$

where k_m is the mass-transfer coefficient in the mobile phase, by definition equal to $D_m\mathrm{Sh}/2R_c$. For coiled columns, Eq. (16) can be used to obtain from Eq. (42)

$$\frac{1}{\mathrm{Pe}_i} = 22\left(\frac{k}{1+k}\right)^2 \frac{1}{\mathrm{Pe}_r(k=0)} \tag{43}$$

which bears a close resemblance to the contribution of the C_m term which amounts to $f(k)(1/\mathrm{Pe}_r(k=0))$. The limit for $k \to \infty$ is $22/\mathrm{Pe}_r(k=0)$, which is somewhat higher than the limit $6/\mathrm{Pe}_r(k=0)$ of the C_m term. For a normal case where $k = 1$, $C_i \approx C_m$, leading to a doubling in plate height but with the same functional dependence on velocity as for the C_m contribution alone. Thus we conclude that in contrast with straight columns, coiled columns have a C_i term with an opposite velocity dependence to the C_s term which does not possess a limiting property like the latter (Fig. 5).

Types of Coating for HOT Columns

An obvious practical problem to be solved before HOT columns can be applied to high-speed separations in LC is to produce a sufficiently stable layer of stationary phase on the column wall. In view of the high velocities involved, high shear rates occur at the phase boundary. Experience with coated capillaries in GC at high flow rates shows that simple coatings of diverse liquids, held to the wall by weak van der Waals forces, are easily stripped off. Good adherence to the wall can, of course, be obtained by chemically bonding a stationary phase to a glass-walled column, analogous to the popular chemically bonded phases on small silica particles. Apart from the doubtful mechanical strength of glass columns, which should be capable of withstanding pressures up to 500 bar, inadequate retention may occur as a result of a low phase ratio (V_s/V_m).

For a smooth-walled glass column of typical dimensions ($L = 772$ cm, $R_c = 0.0125$ cm) and making the reasonable assumption of two active OH-sites per $(\mathrm{nm})^2$ which are capable of forming a bond (*35*), the amount of bonded phase is $(2\pi R_c L)2 \times 10^{14}/N_A = 2 \times 10^{-8}$ mole. For an assumed molar volume of 200 cm^3/mole, we find the phase ratio $V_s/V_m = 10^{-5}$, which is far too low to expect any significant retention. Thus, in

obtaining reasonable capacity factors of about unity with chemically bonded phases, at least a 10^3-fold increase in surface area should be effected. Whether this can be achieved by etching techniques is being studied.

The surface area is certainly high enough if we apply a stable layer of small porous particles to the column wall, which suggests that SCOT-type columns are most promising. For example, the use of silica particles permits not only chemical bonding of a phase but also classical coating with a liquid phase and even direct use of the particles as an adsorbent.

A basic difficulty here is the commonly irregular shape and polydisperse character of the particles, which cause a varying particle density along the column wall. How stringent the requirement of constant particle density is can be simply seen from a model column in which a monolayer of particles is arranged in parallel rows. For liquid-phase-coated particles we consider the amount of stationary phase per row equal to the total particle volume. Differences in the amounts of stationary phase present per row are then proportional to the differences in particle densities. If the densest row consists of n particles of size d_p and the least dense row contains m particles, the corresponding difference in retention times can be calculated.

Assuming this difference to be four times the spread (σ_t) in residence time, we find that the plate height $H = \sigma_z^2/L$, with $\sigma_z = (\bar{u}/1 + k)\sigma_t$, is

$$H = \frac{1}{16} \frac{K^2 d_p^2 L}{R_c^2 (1 + k)^2} \left(\frac{n - m}{n} \right)^2 \tag{44}$$

If we wish to limit this contribution to, say, less than 10% of the total plate height, with $H = 10^{-4}L$ for a required number of plates of 10^4, the following requirement for the allowed spread in the number of particles per row results:

$$\frac{n - m}{n} < \frac{1.3 \times 10^{-2}}{K} \frac{R_c}{d_p} (1 + k) \tag{45}$$

Regarding the particles as a porous adsorbent with a specific surface area a cm^2/g, analogous reasoning yields

$$\frac{n - m}{n} < \frac{1.3 \times 10^{-2}}{\rho a K} \frac{R_c}{d_p} (1 + k) \tag{46}$$

where ρ is the free-fall density. Reasonable estimates for the parameters in Eq. (45) are: $K = 100$; $V_m = 5$ cm^3; $R_c = 0.0125$ cm; $L = 10^4$ cm, and $d_p = 5 \times 10^{-4}$ cm, leading to $k = 4$ and $(n - m)/n < 0.16$. For the

case of adsorption with the same R_c, L, and d_p as above and furthermore $\rho = \frac{1}{4}$ g/cm^3, $a = 50 \times 10^4$ cm^2/g, and $k = 1$ (i.e., $K = 2 \times 10^{-4}$ cm), we find from Eq. (46) $(n - m)/n < 2.6 \times 10^{-2}$.

Thus in both situations a spread of only a few percent in particle density is allowed, which is a difficult practical requirement. Although smaller particle sizes relax this requirement (see Eqs. 45 and 46), particles smaller than 5 μm are difficult to obtain and to handle. To our mind, therefore, in situ formation of very small porous particles (or layers), e.g., by carbonization of methylene chloride, acetylene, or sugar, offers a real possibility of meeting the requirements of homogeneous particle distribution.

As carbonization is often used as a deactivation method for suppressing adsorption (*36*), the carbon deposit must be activated with CO_2 or H_2O at high temperatures (*37*) in order to obtain retention by adsorption.

The carbonaceous layer may also be used as a carrier for a liquid phase, which has been proved with the Grob method (*38*) in capillary GLC.

A special type of SCOT column that may prove useful is the recently developed whisker-walled open-tubular (WWOT) column (*39*). Here C_s terms of typically 5×10^{-4} sec are measured in GLC experiments, approaching the required values for HOT columns (see Fig. 5).

Another possibility is to prepare PLOT-type columns, e.g., by static coating of a slurry of graphitized carbon black (*40*, *41*).

EXPERIMENTAL

Apparatus

The home-made liquid chromatograph consisted of a high-pressure and high flow-rate pneumatic amplifier pump (Tracor 5000), a Waters U6K injector, and a thermostatted water bath that maintained the column at 25.0°C. Two detectors were used, a UV detector (Waters model 440) and a home-made conductometric one for ionic substances. The detector signal was recorded on a Servogor RE571 recorder, used as a reference trace, and at the same time stored in digital form on a cassette tape with a maximum sampling rate of 10 sec^{-1}. At high velocities, where less than a hundred data points per peak are stored, use was made of a galvanometric recorder (SE-Oscillograph 3006/DL) capable of handling sampling frequencies up to 10 kHz without distortion.

The measuring cell of the conductometric detector was carefully designed with regard to dead volumes, even avoiding the slightest changes

in diameter of the flow channel. From our own experience and the literature (*42*) it is known that such changes in diameter generate eddies that have a very bad residence time distribution. Thus, in fact, the measuring cell with its connecting lines should be designed as an extension of the column, with an identical inner diameter. The cell is made of Perspex into which a cylindrical hole is drilled with a diameter equal to the outside diameter of the column tubing.

Two connecting lines consisting of column tubing are attached such that in the center of the cell the metal connecting lines are separated by an isolating spacer ring about 1 mm thick and a central hole whose diameter is again equal to the inner diameter of the tubing. The connecting lines and spacer are glued into place with epoxy glue. The cell and the simple electric circuitry are depicted in Fig. 6. Use of a 69-V battery and a 250-Ω resistance leads to a signal-to-noise ratio which is better by a factor of about 100 than with the commercial conductometer we used before (Philips PW 9501). The response time of the complete detector device was 0.5 msec.

Data Interpretation

All dispersion measurements are expressed in dimensionless axial Peclet numbers based on the column radius (Pe_r) and the dimensionless velocity $v = ReSc$. From recorded peaks the first moment, μ_1, and the square root of the central second moment, σ, were determined either by hand, partitioning recorded peaks into at least 30 parts, or by computer calculation with stored data on a cassette tape as the input. Replacing the residence time, t, in the definition of plate height, $H = L(\sigma/t)^2$, by the first

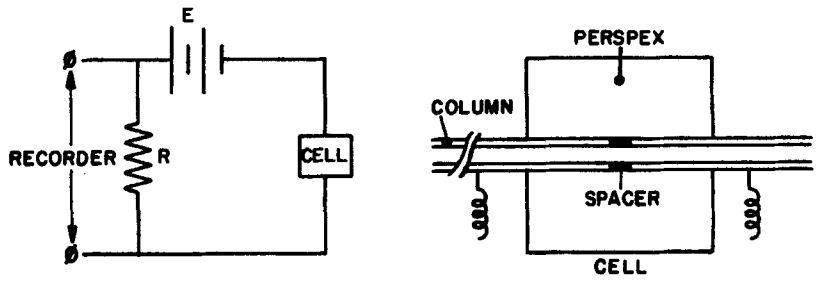

FIG. 6. Conductometric detection device.

moment, μ_1, inverse Peclet numbers can be found from

$$\frac{1}{\mathrm{Pe}_r} = \frac{H}{4R_c} = \frac{L}{4R_c}\left(\frac{\sigma}{\mu_1}\right)^2 \tag{47}$$

Where possible, the mobile phase velocity, $\bar{u}$, was found by weighing the eluate continuously on an electronic balance (Mettler PE 162), the signal from which was also recorded digitally on the cassette tape. At high velocities, at which weighing became impractical, we calculated the linear velocity from the residence time in terms of the first moment

$$\bar{u} = L/\mu_1 \tag{48}$$

which differed slightly from the value obtained by weighing at the lower velocities.

Column Preparation

Commercially available stainless-steel and silver tubing was used as the column material. These columns were equipped with Hoke fittings so that low-dead-volume connections could be made with injection and detection devices. Internal diameters ranged from 0.025 to 0.080 cm, determined by the difference in weight between the empty column and the column filled with distilled water. Column radii, determined from the pressure drop-flow relation and calculated with the Poiseuille equation for low velocities, agreed to within 2% with the value obtained by weighing.

SCOT-type columns were prepared by first applying a sticky liquid film to the column wall by a dynamic coating technique. We tried a number of liquids with hardening properties, such as gelatine, epoxy glues, and transparent lacquers, in suitable solvents. The lacquer yielded the best spreading on metal testplates. Application of the glue as a 10% solution, evaporation of the solvent, and subsequent transport of particles of the support material by a fast gas stream gave the best results. Blowing through a plug of particles at 30 to 100 bar or applying a vacuum at the end of the column gave good results, although the reproducibility in the latter method was poor. All trials in which the support particles were suspended in the glue solution with subsequent coating of the column failed. As the support materials we used silica particles, irregularly shaped 5-μm particles (Merckosorb SI 60) and 10-μm spherical particles (Merckosorb SI 100). Trials with the spherical particles, however, were not successful. Hence, all results reported on SHOT columns in the next section were obtained with SI 60.

RESULTS AND DISCUSSION

Flow Phenomena

These phenomena will be discussed fully elsewhere (*22*), but some relevant results on the velocity dependence of the secondary flow velocity, u_s, and the pressure drop will be discussed briefly here. These results have been used already in the theoretical part to arrive at the final dispersion relations.

Secondary Flow Velocity

A simple way to obtain the relationship between u_s and the average velocity, $\bar{u}$, is to use dye tracer experiments in glass and transparent plastic tubes. By continuous injection of methylene blue in water, one can visualize the actual streamlines. The time needed to traverse the cross section of the tube is a direct measure of u_s. For instance, at high velocities u_s equals $2(R_c - \delta)t^{-1}$. For the central line AB in Fig. 1 we observed (*22*) that the results can be described by

$$\frac{u_s R_c}{\nu} = \frac{\mathrm{De}^{1/2}}{1 + \dfrac{120}{\mathrm{De}^{3/2}}}, \qquad 0.1 < \mathrm{De} < 10^4 \tag{49}$$

over 5 decades in velocity. Equation (49) was used to eliminate u_s from the expressions for D_s in the theoretical part. The experimental relation, Eq. (49), has two important velocity asymptotes: at the lower velocities

$$\frac{u_s R_c}{\nu} = \frac{\mathrm{De}^2}{120} \qquad (\mathrm{De} < 20) \tag{50}$$

and at high velocities:

$$\frac{u_s R_c}{\nu} = \mathrm{De}^{1/2} \qquad (\mathrm{De} > 100) \tag{51}$$

Equation (50) is in very good agreement with theoretical calculations on u_s (*22*) using the velocity profile of Dean (*12*), resulting in

$$\frac{u_s R_c}{\nu} = \frac{\mathrm{De}^2}{114} \tag{52}$$

The same applies to calculations on the Mori profile at high velocities:

$$\frac{u_s R_c}{\nu} = 0.966\mathrm{De}^{1/2} \tag{53}$$

in very good agreement with the experimental results, Eq. (51). This is an indication that both the Dean and Mori profiles are reliable descriptions of the velocity profile at low and high velocities, respectively.

Using Eq. (50) for the lower velocities and our earlier estimate for D_s being u_sR_c or $(D_s/D_m) = (u_sR_c/\nu)\mathrm{Sc}$, we have

$$\frac{D_s}{D_m} = \frac{\mathrm{De}^2\mathrm{Sc}}{120} \qquad (\mathrm{De} < 20) \tag{54}$$

which differs by a factor of 1/2.26 from the present result (Eq. 5 in Table 1). In all other velocity regions the agreement is even worse. For example, at intermediate velocities D_r/D_m even becomes a constant (6.39), after Eq. (6), in satisfactory accordance with the rough estimate of about 4 (see the section entitled "Radial Dispersion in Helices") based on the division of the column into two halves.

The high-velocity cases (Eqs. 7 and 8) were originally derived in terms of u_s as (*22*)

$$\frac{D_s}{D_m} = \frac{u_sR_c}{\nu}\mathrm{Sc}\frac{16/3\pi^2}{(\delta/R_c)} \qquad \text{(gases)} \tag{55}$$

and

$$\frac{D_s}{D_m} = \frac{32}{3}\left(\frac{u_sR_c}{\nu}\right)^{1/2}\Big/(\delta/R_c)^2 \qquad \text{(liquids)} \tag{56}$$

Both expressions indicate that the former assumption, $D_s = u_sR_c$, is not obeyed. It must be remarked that D_s in Eqs. (55) and (56) is strongly influenced by the boundary layer thickness, δ, which in turn is dependent on velocity, as shown by Eq. (22). In our earlier work we wrongly supposed δ to be a constant.

Pressure Drop and Friction Factor

Many experiments and predictions on friction factors have been reported in the literature, but they are valid only for restricted velocity ranges. In this work, experiments on friction factors for 5 decades in velocity have been carried out.

Friction factors, f, describe the relation between pressure drop and velocity and are defined as $f = (\Delta p/\rho\bar{u}^2)/(R_c/L)$ for open tubes. In straight open tubes, the well known relation

$$f_0 = 16/\mathrm{Re} \qquad (\mathrm{Re} < 2300) \tag{57}$$

holds (*23*). For coiled tubes, the present experimental data for nitrogen flowing through a variety of columns with different radii and aspect ratios

can be fitted by the function

$$\frac{f}{f_0} = 1 + \alpha(\mathrm{De}) = 1 + \frac{0.107\mathrm{De}^{1/2}}{1 + \frac{12}{\mathrm{De}^{1/2}} + \frac{700}{\mathrm{De}^{3/2}}} \tag{58}$$

Again, as for u_s, the asymptotic behavior is in excellent accord with theory, e.g., with the relation $(f/f_0) = 0.1064\mathrm{De}^{1/2}$ given by Adler (*14*). Experiments by other workers (*12–21*, *24*, *25*, *30*) on both gases and liquids are equally well described by Eq. (58).

From this result and the analogous situation for u_s we conclude that the theoretical descriptions of velocity profiles at low velocities [Dean (*12*)] and high velocities [Adler (*14*)] are reliable. Recently, Wong et al. (*26*) doubted the assumed shape of these velocity profiles that had been applied already in our earlier work (*7*, *8*). The experimental evidence given here provides a strong argument for their reliability.

Detector Requirements

The potential of HOT columns to generate very high numbers of plates in short times can only be realized if extra column band broadening is limited. Here a serious practical problem arises as presently available detectors, although having reasonable dead volumes of about 5 μl, always suffer from long response times, τ, of the order of 0.5 sec. Time constants have a comparable influence to standard deviations on spreading (*42*):

$$\sigma^2 = \sigma_c^2 + \tau^2 \tag{59}$$

where σ_c^2 represents the variance generated in the column. Thus τ should be restricted to, say, $\frac{1}{4}\sigma_c$ in order to be of acceptable influence. This means that $(\tau/t) < (1/4n_{th}^{1/2})$, so if we wish to generate 10^4 plates in 1 sec, τ is restricted to 2.5 msec. This goal can be reached in GC by using adapted flame-ionization detectors and electrometer amplifiers, but LC detectors are problematic in this respect. In our opinion, electrochemical detectors offer the best prospects, illustrated by $\tau = 0.5$ msec for the simple home-made conductometric detector described in the "Experimental" section above.

AXIAL DISPERSION WITHOUT RETENTION

Nonliquids

Although our aim was to investigate the behavior of liquids, the theory also yielded relations for fluids with low Sc numbers such as gases and

supercritical systems (gases: Sc < 4; liquids: Sc > 100; supercritical: 2 < Sc < 200). Some relevant experimental results, depicted in Fig. 7 after suitable pressure corrections (*51*), will be discussed here.

First, it is seen that notwithstanding careful corrections for extra column broadening, the experiments on straight tubes do not follow Taylor's relation $(1/\mathrm{Pe}_r) = (v/192)$, but rather $(1/\mathrm{Pe}_r) = (v/100)$. The most probable explanation may be that common peak position and peak width were used in all experiments in Fig. 7 (except for line *g*), instead of the first and second moments that should be taken when the peak shapes were non-Gaussian. Indeed, line *g*, for which moments were used, agrees very well with $(v/192)$ for the lower velocities. Other authors (*51–53*) found deviations from the Taylor equation for the same reason, without noticing the fact at that time.

The present theory predicts that deviations from straight-column dispersion should occur for $\mathrm{De}^2\mathrm{Sc} > 30$. This means that for $\lambda = 1/14$ (Cases *a*, *b*, and *c* in Fig. 7), $\mathrm{ReSc} > 20$, as is shown by the experiments in Fig. 7.

At somewhat higher velocities, Eq. (31) (Table 2) should apply. It can be seen that functional predictions ($1/\mathrm{Pe}_r$ is proportional to $v^{1/2}$ and higher for higher Sc) are confirmed by Cases *a*, *b*, and *c*, but numerically the experimental dispersion is higher than predicted by about a factor of 3. Although a factor of 2 can be attributed to the evaluation of Pe_r via common peak parameters instead of moments, it seems that the numerical constants in our theoretical model are only approximative. The same will be observed for liquids.

At high velocities the intersection of the lines represented by Eqs. (31) and (33a) predicts a maximum of the inverse Pe number or inverse plate number at

$$\mathrm{Re} = \frac{4.5 \times 10^3}{\lambda^{1/2}\mathrm{Sc}^{4/3}} \tag{60}$$

For Cases *d* and *e* in Fig. 7, this leads to $v = 3.7 \times 10^4$ and 3×10^4, respectively, i.e., quite near, although higher than, the observed maxima (6×10^3 in Fig. 7).

We observe, furthermore, that Cases *d* and *e* differ little in Pe_r over the whole velocity range. This is predicted by Eq. (33a), which shows a decrease in dispersion for higher Sc numbers (leading to a factor of $(9.5/1.75) \cong 5$ in comparing *d* with *e*) but an increase for smaller λ (leading again to a factor of $(1/60)/(1/307) \cong 5$). This gives some confidence in the

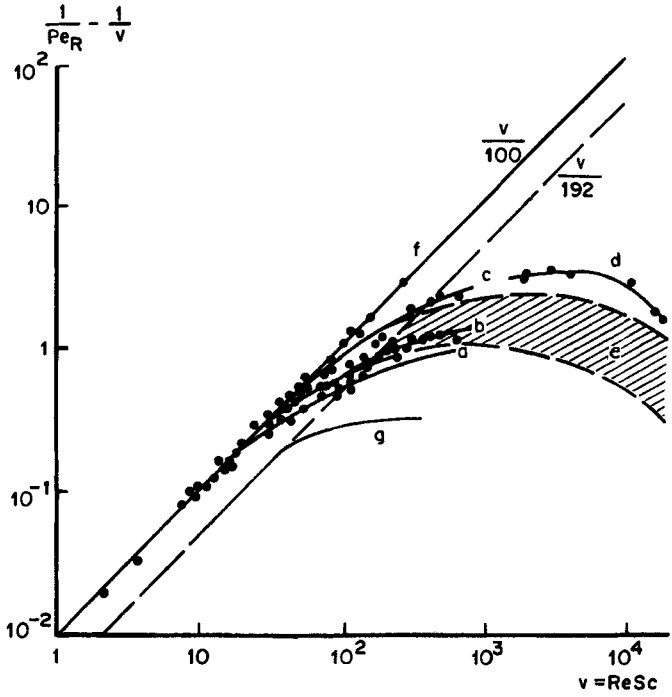

FIG. 7. Experimental axial dispersion with gaseous and supercritical mobile phases in straight tubes and HOT columns. (*a*) This work, Sc = 0.254. (*b*) This work, Sc = 0.685. (*c*) This work, Sc = 1.432. For (*a*), (*b*), and (*c*), $\lambda = 1/14$ and mobile phase N_2. (*d*) Sie and Bleumer (*43*), Sc = 9.5, $\lambda = 1/30$; mobile phase: supercritical pentane. (*e*) Van Andel et al. (*44*), Sc = 1.75, $1/104 < \lambda < 1/30$. (*f*) This work, straight columns, Sc and λ as in (*a*), (*b*), and (*c*). (*g*) Kolk (*50*), Sc = 1.75, $\lambda = 1/9$, moments.

present theory which is also supported by similar recent experiments for gases by Wong (*26*) and Kolk (*50*).

Liquids at Low Velocities

This case should be described, for instance, by Eq. (5) (Table 1), i.e., in the range $De^2Sc < 2300$ a linear relation between $\xi = (D_r/D_m) - 1$ and the velocity parameter De^2Sc should be observed. This was confirmed by our own experiments and by recalculated literature data, as illustrated in Fig. 8. Here Sc ranges from 0.66 for gases, through Sc $\cong$ 10 for supercritical systems, to Sc = 500 for liquids, and even Sc $\cong 10^4$ for macromolecular solutions. The linear relation between ξ and De^2Sc should hold

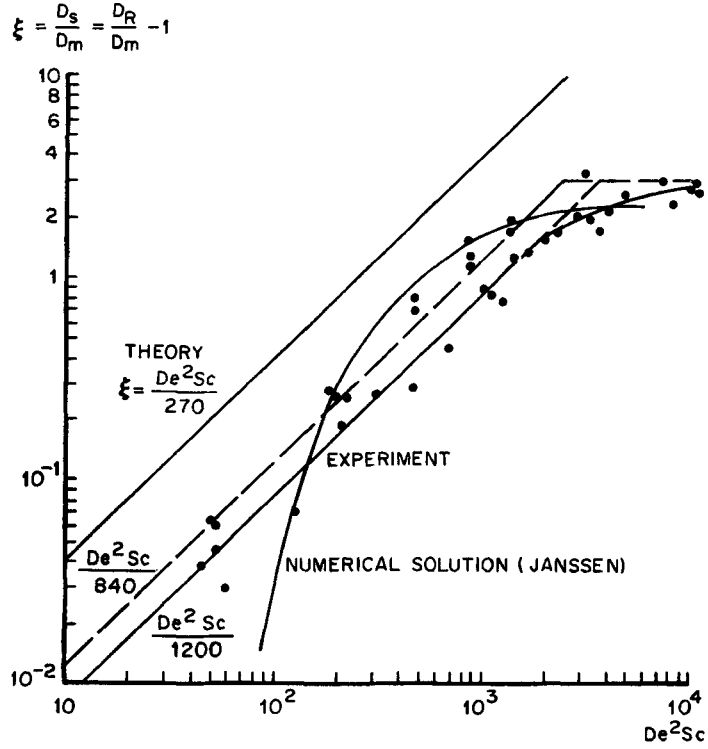

FIG. 8. Velocity dependence of radial secondary flow dispersion from own experiments and recalculated literature data (*43–49*).

up to $De^2Sc = 2300$ (Eq. 4) and indeed breaks down at $De^2Sc > 2 \times 10^3$, as shown by the experimental points in Fig. 8.

In the lower velocity limit, deviation from straight-column dispersion becomes observable (e.g., $\xi = 0.02$) at velocities higher than that corresponding to $De^2Sc = 30$, the same as for gases and predicted in the Appendix. However, the numerical value of the proportionality constant in the relation between ξ and De^2Sc does not agree with the predicted constant (1/1200 and 1/270, respectively), as was found for gases.

Recalculated literature data are mostly based on common peak parameters instead of moments and can be described by $\xi = De^2Sc/840$ instead of $\xi = De^2Sc/1200$ ($De^2Sc < 2 \times 10^3$).

At velocities higher than that corresponding to $De^2Sc \cong 2 \times 10^3$, where, after Eq. (6) (Table 1), ξ should attain a constant value of about 5, a constant is indeed approached in Fig. 8, having a value of about 3. Thus, in both limiting situations in Fig. 8, the predicted velocity dependence is confirmed, whereas the theoretical and experimental numerical constants deviate. The predicted constants are easily adapted as they depend very much on the way in which the cross section is divided into wall and core regions (see the section entitled "Radial Dispersion" and Ref. *22*). Functional forms are not influenced, so we conclude that the model presented is basically correct and only needs numerical corrections. Apart from the justifications of the model already discussed, it is observed from Fig. 8 that at $De^2Sc > 5 \times 10^3$ the same constant value for ξ of about 3 is approached, irrespective of the aspect ratio, Sc number, etc. Indeed, this should be the case as the model uses the underlying mechanism of subdivision of the original column into two parallel ones.

Figure 8 shows, furthermore, that the velocity dependence predicted by the present theory is in much better agreement with the experimentally observed dependence than the numerically obtained solution to the mass balance, Eq. (9), of Janssen (*24*, *25*). Based on data points calculated from moments, a good fit for the whole velocity range in Fig. 8 is given by

$$\xi = \frac{D_r}{D_m} - 1 = 3\left[1 - \frac{30}{(De^2Sc)^{1/2}} + \frac{3600}{De^2Sc}\right]^{-1} \qquad (61)$$

Liquids at Intermediate and High Velocities

Here a gradual change from the dispersion behavior predicted by Eq. (32) into that predicted by Eq. (34a) (Table 2) should be observed. Figure

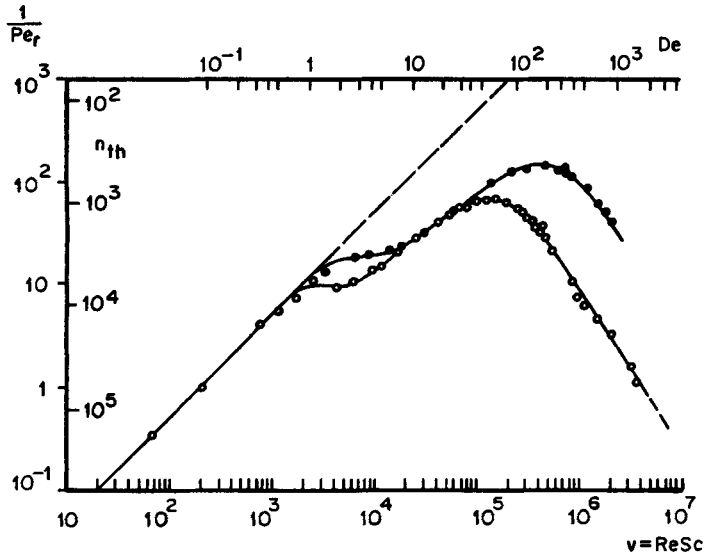

FIG. 9. Axial dispersion in a HOT column without retention. $\lambda = 1/20$, $R_c = 0.04$ cm, and $L = 1007$ cm. (○) KI in water (25°C), Sc = 525; (●) Dobanol (Teepol) in water (25°C), Sc = 2450.

9 illustrates how measurements on two ionic substances in water, using moments, indeed show a maximum in $1/Pe_r$ at $v > 10^5$. The maximum predicted from the intersection of Eqs. (32) and (34a)

$$Re = \frac{545}{\lambda^{1/2} Se^{0.57}}$$

corresponds to $v = 3.6 \times 10^4$ for Sc = 525 and to $v = 7 \times 10^4$ for Sc = 2450, both of which are near to, but lower than, the measured values in Fig. 9. Again, numerical deviations between theoretical and experimental values occur, especially at velocities above those where the maximum in $1/Pe_r$ is reached. Then Eq. (34a) predicts inverse Pe numbers which are lower by about a factor of 10 than the observed ones. However, the steep decline at higher velocities is confirmed, although the experimental data show an even steeper slope ($-3/2$) than is predicted by Eq. (34a) (-1). The theory should be refined here, but in any event the predicted trends are applicable to very high-speed LC.

Because we carried out experiments up to very high velocities, it can be seen that the agreement between experiment and theory when the modified

Mori profile was used (Eq. 34b) is even worse (compare slope $-\frac{1}{2}$ in Fig. 3 with Fig. 9). This result casts doubt on the reliability of Mori's analytical expression for the velocity profile at high velocities. Experimental results on liquids in the literature (*45*) correspond to velocities only as high as $v = 10^6$. These results, recalculated in terms of Pe numbers, fall in the same region as those reported in Fig. 9, but do not agree quantitatively. First, no intermediate region parallel to the Taylor line is observed and second, the trend at high velocities, but with $v < 10^6$, is much less declined than those in Fig. 9. Although $v < 10^6$ is not sufficiently fast for a reliable impression of the limiting slope, the mentioned results at intermediate velocities indicate that those experiments were not reliable enough, possibly owing to the strong extra-column band broadening requirements.

One may compare the high-velocity results of Fig. 9 with those reported for zone dispersion in very high-speed turbulent flow (*54–56*) in straight columns. It can be concluded then that the present HOT columns yield the same small axial dispersion accompanied by a reasonable pressure drop (still laminar flow) and more attractive residence times (by the lower axial velocities).

Although only the sharply declining part of the dispersion characteristics in Fig. 9 is of direct use for the development of very high-speed LC, the behavior in the intermediate velocity region can be utilized in normal LC. Here a more or less constant gain in axial dispersion by a factor of 3 to 4 compared with the straight column is observed. It is well known that in both GC and LC measurable contributions to zone broadening often occur, arising from unavoidable connecting lines between the column and the injection and detection devices. Obviously this contribution can be reduced by a factor of 3 to 4 by simply coiling the connecting lines as tightly as possible. Even if greater lengths are necessary, then this is to be preferred provided that it is below a factor of, say, 2. Applying this expedient in our experience often causes especially early peaks with low capacity factors ($k < 1$) to be less broadened.

AXIAL DISPERSION AND RETENTION

Columns Coated with Liquid Films

In order to test the shear-off stability of classical film coatings, stainless-steel capillaries were coated by a dynamic coating procedure with tri-*n*-octylamine (TNOA) and β,β'-oxydipropionitrile (ODPN) as stationary phases. With TNOA we tried to perform ion-pair partitioning as described

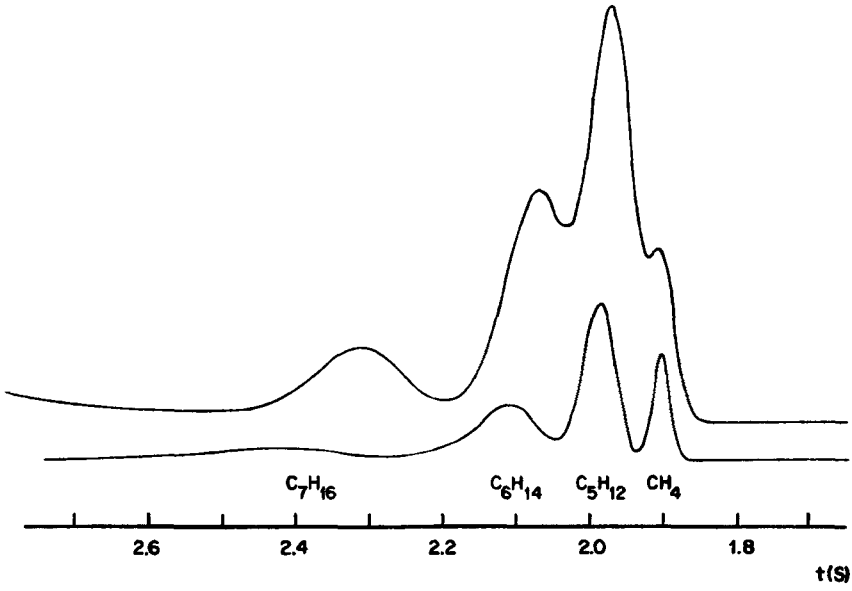

FIG. 10. Comparison of separation efficiency in GC. Upper trace: straight column. Lower trace: same column but coiled. $L = 10$ m and $R_c = 0.013$ cm. Stationary phase: squalane.

by Kraak (*57*). The high water content of the mobile phase here allowed the use of a conductometric detector. Although sufficient retention could be obtained, supporting the discussion on the expected capacity factors (see the section entitled "Retention and Axial Dispersion"), the peak shapes were poor (with tailing probably caused by a slow step in the ion-pair formation), whereas near $v = 10^5$ complete loss of the stationary phase resulted. The same applied to ODPN columns. The stability of liquid-coated capillary columns for GC is much better, possibly because of different kinematic viscosities of gases compared with liquids. Hence GLC can be relatively easily applied up to very high velocities, whereas flame-ionization detection does not offer any great difficulties. By way of illustration, Fig. 10 represents a model separation of some alkanes on squalane as the stationary phase. Notwithstanding the low viscosity of squalane, the liquid film is stable up to linear velocities of 10^4 cm/sec (outlet conditions). In our experience, more viscous stationary phases (OV's, SE, etc.) are much more resistant to shearing off. Figure 10 clearly shows the beneficial effect of coiling on resolution in open-column chromatography.

Again using GC for *n*-hexane at 120°C on OV-1 as the stationary phase,

we measured $C_s = 1.1 \times 10^{-4}$ sec, which is in the desired range (cf. Fig. 5). The C_m term well fitted the experiments using the retention function $f(k) = (1 + 3k + 4k^2)/(1 + k)^2$. The disagreement with the predicted function (Eq. 25) again gives rise to criticism of the Mori velocity profile which is used to find Eq. (25).

Columns Coated with Particles

The shear-off stability of SHOT columns with silica particles glued to the wall as well as columns with a carbon layer is very good indeed. Columns coated with silica particles, however, show plate heights which cannot be explained by $f(k)$ alone, especially as GC experiments (see preceding section) reveal that $f(k)$ may be even smaller than the value predicted by Eq. (25). Figure 11 clearly illustrates this. Although the retained substances exhibit the desired trend to increasing efficiency at high velocities, the loss in efficiency compared with the nonretained substances is too great, especially at high velocities. This may be caused by a high C_s term and/or the nonuniform particle density (discussed in the section entitled "Types of Coating for HOT Columns"). The latter imperfection actually shows up in electron microscope photographs (Figs. 12A and 12B), and can be of two kinds, a large-scale irregularity caused by the structure of the column wall and a random irregularity on a smaller scale which even includes regions several particle diameters in size that are completely free of particles. The large-scale irregularity can be prevented by using smooth-walled columns made of materials such as silver, precision-bore stainless steel, and glass; the small-scale one is thought to be influenced by particle shape (regular or not) and type of transport of the particles during the glueing process (fast or slow gas stream). The silica can be used as an adsorbant as such but also as a support material for liquid coating. In both situations, using ODPN in the coated column, the plate height was approximately the same for the same capacity factor. This result indicates that the same broadening mechanism governs plate heights in both cases, viz., the nonuniform particle density. Commercially available SCOT columns and carbon-coated PLOT columns and alkali-etched glass columns (*5*, *58*), among other types, will be tested in the near future.

CONCLUSION

In this work the potential of HOT columns for LC has been investigated. Apart from numerical deviations, predicted efficiencies in different

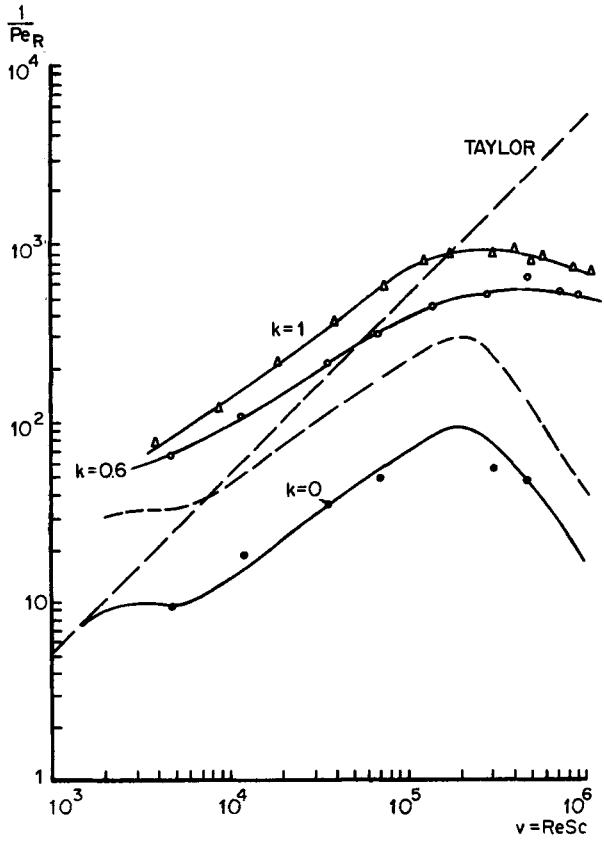

FIG. 11. Axial dispersion in a silica-coated silver HOT column for retained and unretained compounds. $L = 11$ m, $R_c = 0.025$ cm, and $\lambda = 1/40$. $k = 0$ (toluene) and $k = 0.6$ (aniline), both in LSC-mode. $k = 1$: phenol in LLC-mode with ODPN coated on silica as the stationary phase. Mobile phase in all cases: isooctane + 0.1% tetrahydrofurane. (– –) theory including $f(k)$ for $k = 0.6$.

FIG. 12. Scannng electron microscope images of the coated wall of a stainless steel HOT column. Particles: Silica SI-60 (5 μm).

velocity ranges are confirmed. As a practical result, at low velocities it is recommended that all connecting lines in GC and LC apparatus should be coiled as tightly as possible. Further, an improved correction for coiling effects in the determination of diffusion coefficients is given (see the Appendix), with the aim to achieve determination times of the order of minutes even for slowly diffusing substances like macromolecules. At high velocities the predicted separation speed in HOT columns used for LC increases with the velocity squared, whereas the experiments revealed an even higher power in velocity, viz., 5/2 (see Fig. 9). Values of 10^4 to 10^5 plates per second can be reached at pressures already available for packed columns (which only yield 10^2 plates/sec). Compared with turbulent-flow chromatography, HOT columns yield the same efficiency at lower pressures and more practical residence times. Thus we consider that open columns can play a promising role in the future of LC, especially where high efficiencies and short analysis times are needed (process control). The short times pose problems, yet to be solved, in the fields of detectors and coatings.

APPENDIX: RAPID DETERMINATION OF DIFFUSION COEFFICIENTS

The foregoing theory was tested and applied most easily either with nonretained substances ($k = 0$) or in the absence of a stationary phase. Under these conditions, zone spreading is a direct measure of the diffusion coefficient. Consequently, on the basis of the Taylor equation, the chromatographic band-broadening technique has been developed into a method for determining diffusion constants in gases as well as in liquids (*46*). Although several authors recognized the consequences of the commonly coiled geometry of the column, they all underestimated the influence of secondary flow on dispersion. Only Ouano and Carothers (*47*, *48*) recommend a method to correct for coiling effects. Their method is, however, open to criticism as will be shown.

At velocities corresponding to $v > 100$, axial dispersion of a nonretained solute zone can be interpreted with the C_m term only. In terms of dispersion coefficients, Eq. (27) can be written as

$$\frac{D_z}{D_m} = \kappa \frac{R_c^2 \bar{u}^2}{(D_r/D_m)} \tag{A1}$$

The Taylor equation is a limiting case of Eq. (A1) for straight columns where $\kappa = 1/48$ and $D_r = D_m$. Most experiments, however, are carried

out in helically coiled tubes, which means that even for low velocities, where $\kappa = 1/48$ can be used, $D_r \neq D_m$ and the relations from Table 1 should be applied. Assuming that secondary flow effects become observable in the experiments if D_s amounts to more than 10% of D_m (i.e., $\xi = (D_s/D_m) > 0.1$), we have from Eq. (5) the condition

$$De^2Sc > 30 \tag{A2}$$

Figure 8 shows this to be true experimentally. Thus reliable diffusion constants from the Taylor equation can only be obtained in straight columns or with very low velocities ($De^2Sc < 30$) in the more practical coiled columns.

For example, applying practical velocities corresponding to Re = 10 (i.e., $\bar{u} = 2$ cm/sec in a column with $R_c = 0.025$ cm) $De^2Sc < 30$ implies for liquids (Sc = 500) that the aspect ratios λ should be smaller than 1/1667, which is just as impractical as in a straight column. The opposite case, choosing a practical value for λ, say $\lambda = 1/50$, requires the application of velocities corresponding to Re < 1, leading to very long residence times, especially for substances with high Sc numbers such as macromolecules. In the literature we observe that even for normal liquids with Sc $\approx$ 500, the reported experimental conditions are not within the range imposed by $De^2Sc < 30$. In those cases the combination of Eqs. (5) and (A1) provides a more reliable means of finding D_m from dispersion experiments. Equation (61), which is based on experiments adapting the constant in the theoretical Eq. (5) to a reliable value (1200), is recommended, however, and is to be applied even up to $De^2Sc = 10^4$. As radial dispersion depends quadratically on velocity up to $De^2Sc = 2 \times 10^3$, we conclude that the linear extrapolation of experimental D_r values to zero velocity, suggested by Ouano and Carothers (*47*, *48*) to correct for coiling effects, underestimates the values of D_m.

Purposely using coiled columns in the determination of D_m and applying higher velocities than usual have the advantage of enhanced radial mass exchange, leading to shorter residence times than is permissible in straight columns. Taylor (*59*) introduced a condition for residence time, t, based on the idea that radial exchange should be able to cover the column cross section at least once before elution takes place. In the case where D_r describes radial exchange we now assume, instead of Taylor's $(D_m t/R_c^2) > 1$,

$$\frac{D_r t}{R_c^2} > 1 \tag{A3}$$

Using a certain velocity ($\bar{u} = L/t$), coiled tubes can thus be chosen that are shorter than straight columns by a factor of (D_r/D_m). Alternatively, velocity can be chosen to be higher by the same factor. Up to intermediate velocities, the gain in this factor (D_r/D_m) is limited to a value of 4 to 6 (from experiments and Eq. 5) but at high velocities it is much more pronounced (see Table 1). For instance, for liquids we find from Eqs. (8) and (A3) that

$$t > 8 \times 10^3 \frac{R_c^2}{\mathrm{De}^{3/2}\nu} \tag{A4}$$

This means, e.g., in a column with $R_c = 0.0125$ cm, De = 100, and $\nu = 10^{-2}$, that the residence time, t, has to be at least 0.1 sec. In consequence, it should be possible to obtain diffusion coefficients within minutes, irrespective of Sc number, even for macromolecules ($D_m \approx 10^{-7}$ cm^2/sec). Instead of residence times, the required column length can be calculated from Eq. (A3) as

$$L > \frac{R_c}{2(D_r/D_m)}\mathrm{ReSc} \tag{A5}$$

(for straight columns $D_r = D_m$, so $L > (R_c/2)\mathrm{ReSc}$).

For liquids we have from Eqs. (8) and (A5):

$$L > 4 \times 10^3 \frac{R_c}{\mathrm{De}^{1/2}\lambda^{1/2}} \tag{A6}$$

For the same R_c, De as before and with $\lambda = 1/10$, Eq. (A6) requires $L >$ 15.8 cm. A straight tube operated at the same velocity (Re = 316) already needs $L > 988$ cm for Sc = 500. For slower diffusing molecules (Sc > 500), the required length for straight columns increases linearly with Sc, whereas for coiled columns (Eq. A6) L is independent of Sc. It thus seems that dispersion in HOT columns offers very attractive properties for the rapid determination of diffusion coefficients for solutes ranging from gases to high-molecular-weight substances.

SYMBOLS

a	specific area (cm^2/g)
B	$= 2D_m$, axial molecular diffusion term in plate height equations (cm^2/sec)
c^*	equilibrium concentration
c_m	concentration in mobile phase

C_m	axial dispersion term from mobile phase contributions (sec)
C_i	interfacial resistance term (sec)
C_s	stationary phase contribution to axial dispersion (sec)
$\overline{d^2}$	average squared displacement (cm^2)
d_p	particle diameter (cm)
D_m	molecular diffusion coeficient (cm^2/sec)
D_r	$= D_m + D_s$, radial dispersion coefficient (cm^2/sec)
D_s	secondary flow dispersion coefficient (cm^2/sec)
f	friction factor
$f(k)$	retention function
F_{cf}	centrifugal force
H	$= L/n_{th}$, plate height (cm)
H_m	$= C_m\bar{u}$
H_s	$= C_s\bar{u}$
j	$\cong f/f_0$
k	$= K(V_s/V_m)$, capacity factor
k_m	mass transport coefficient
K	$= c_s/c_m$, partition coefficient
L	column length (cm)
Δp	pressure drop (bar)
r	radial coordinate
R_c	column radius (cm)
t	time (sec)
t_0	$= t_w + t_c$, circulation time (sec)
$u_{z,r,\varphi}$	local velocity in certain direction (cm/sec)
$\bar{u}$	$= L/t$, average linear velocity
u_s	secondary flow velocity (cm/sec)
$V_{m,s}$	volume of mobile and stationary phases (cm^3)
z	axial coordinate

Greek Symbols

$\alpha(\mathrm{De})$	$\cong j - 1$
δ	boundary layer thickness (cm)
δ_f	film thickness
∇^2	$= \nabla_{r,\varphi}{}^2 + (\partial^2/\partial z^2)$
$\nabla_{r,\varphi}{}^2$	$= (1/r)(\partial/\partial r)[r(\partial/\partial r)] + (1/r^2)(\partial^2/\partial\varphi^2)$
κ	velocity profile factor
λ	$= R_c/R_{\mathrm{helix}}$, aspect ratio
μ_1	$\int_0^\infty ct\,dt$, first (time) moment

ν $= \eta/\rho$, kinematic viscosity (cm^2/sec)
ξ $= D_s/D_m$
ρ $= r/R_c$, radial coordinate: sometimes density
σ square root of second central moment (sec)
σ_c standard deviation generated by column processes (sec)
τ response time, time constant (sec)
τ_m exchange time (sec)
φ angle

Dimensionless Numbers

De $= \mathrm{Re}\ \lambda^{1/2}$, Dean number
Nu Nusselt number ($\equiv$ Sh for mass transfer)
Pe_L $= \bar{u}L/D = 2n_{th}$, Peclet number based on length
Pe_r $= (H/4R_c)^{-1}$, Peclet number based on radius
Re $= (2R_c\bar{u}/\nu)$, Reynolds number
Sc $= \nu/D_m$, Schmidt number
Sh $= (2R_c k_m/D_m)$, Sherwood number

Indices

0 straight column

Acknowledgments

Part of this work was done at the Laboratory for Analytical Chemistry of the Technological University Delft, The Netherlands, headed by Dr. L. de Galan. In particular, experiments on gases and flow phenomena were carried out there in close collaboration with Ir. R. T. Wittebrood, now with Shell Internationale Petroleum Maatschappij B.V. Thanks are due to N. van den Hoed for his aid in many experiments on liquids and to Dr. M. E. van Kreveld for critically reading the manuscript.

Notes Added in Proof. Novotny et al.(*60*) recently published an experimental study on coiled columns for LC which qualitatively support the present conclusions. The authors applied nonretarded solutes at low velocities (De<7.5). Interesting results were obtained with packed microcapillary columns which show, however, plate heights exceeding those for open columns by a factor or 2 or more.

Since submitting this paper, more data on retarded solutes in LC have become available which confirm the large broadening reported in this study. The additional plate

height can be described by a C-term which strongly increases in the course of a chromatogram. This points to the presence of an interphase resistance to mass transfer, small or absent in capillary GC and in packed or packed capillary columns. In open columns for LC the effect, also expected to occur in turbulent flow chromatography, can be compensated for by introducing flow of the "stationary" phase. This will be discussed in a future contribution.

REFERENCES

1. B. L. Karger, L. R. Snyder, and C. Horvath, *An Introduction to Separation Science*, Wiley, New York, 1973.
2. J. C. Giddings, *Dynamics of Chromatography*, Dekker, New York, 1965.
3. D. Jentzsch, G. Oesterhelt, E. Rödel, and H.-G. Zimmerman, *Z. Anal. Chem.*, *205*, 237 (1964).
4. C. G. Horvath, B. A. Preiss, and S. R. Lipsky, *Anal. Chem.*, *39*, 1421 (1967).
5. G. Nota, G. Marino, V. Buonocore, and A. Ballio, *J. Chromatogr.*, *46*, 103 (1970).
6. M. J. E. Golay, in *Gas Chromatography 1958* (D. H. Desty, ed.), Butterworths, London, 1958, p. 36.
7. R. Tijssen, *Chromatographia*, *3*, 525 (1970).
8. R. Tijssen and R. T. Wittebrood, *Ibid.*, *5*, 286 (1972).
9. I. Halaśz, Plenary paper presented at the 11th International Symposium on Chromatography, July 5–9, 1976, Birmingham, England.
10. G. I. Taylor, *Proc. R. Soc. (London)*, *A219*, 186 (1953).
11. R. Aris, *Ibid.*, *A235*, 67 (1956); *A252*, 538 (1959).
12. W. R. Dean, *Philos. Mag.*, *4*, 208 (1927); *5*, 682 (1928).
13. H. C. Topakoglu, *J. Math. Mech.*, *16*, 1321 (1967).
14. M. Adler, *Z. Angew. Math. Mech.*, *14*, 257 (1934).
15. H. Ito, *J. Basic Eng., Trans. ASME, D81*, 123 (1959); *Z. Angew. Math. Mech.*, *49*, 653 (1969).
16. Y. Mori and W. Nakayama, *Int. J. Heat Mass Transfer*, *8*, 67 (1965); *10*, 37, 681 (1967).
17. W. R. Dean and J. M. Hurst, *Mathematika*, *6*, 77 (1959).
18. L. C. Truesdell and R. J. Adler, *AIChE J.*, *16*, 1010 (1970).
19. L. R. Austin and J. D. Seader, *Ibid.*, *19*, 85 (1973).
20. D. Greenspan, *J. Fluid Mech.*, *57*, 167 (1973).
21. W. M. Collins and S. C. R. Dennis, *Q.J. Mech. Appl. Math.*, *2*, *28*, 133 (1975).
22. R. Tijssen, Ph.D. Dissertation, In Preparation, Technical Univesity Delft.
23. R. B. Bird, W. E. Stewart, and E. N. Lightfoot, *Transport Phenomena*, Wiley, New York, 1960, p. 559.
24. L. A. M. Janssen, *Chem. Eng. Sci.*, *31*, 215 (1976).
25. L. A. M. Janssen, Ph.D. Dissertation, Delft, 1976.
26. A. K. Wong, B. J. McCoy, and R. G. Carbonell, *J. Chromatogr.*, *129*, 1 (1976).
27. M. N. Özisik and H. C. Topakoglu, *J. Heat Transfer, Trans. ASME, C90*, 313 (1968).
28. C. E. Kalb and J. D. Seader, *Int. J. Heat Mass Transfer*, *15*, 801 (1972).
29. A. N. Dravid, K. A. Smith, E. W. Merrill, and P. L. T. Brian, *AIChE J.*, *17*, 1114 (1971).

30. P. S. Srinivasan, S. S. Nandapurkar, and T. A. Holland, *Trans. Inst. Chem. Eng.*, *46*, CE 113 (1968).
31. M. A. Khan, in *Gas Chromatography 1962* (M. van Swaay, ed.), Butterworths, London, 1962.
32. G. S. F. Hazeldean and R. P. W. Scott, *J. Inst. Pet.*, *48*, 380 (1962).
33. G. J. Krige and V. Pretorius, *Anal. Chem.*, *35*, 2009 (1963).
34. M. R. James, J. C. Giddings, and H. Eyring, *J. Phys. Chem.*, *68*, 1725 (1964).
35. H. Hemetsberger, W. Maasfeld, and H. Ricken, *Chromatographia*, *9*, 303 (1976).
36. D. Zoccolillo and A. Liberti, *J. Chromatogr.*, *77*, 69 (1973).
37. M. Smísek and S. Cerný, *Active Carbon*, Elsevier, Amsterdam, 1970.
38. K. Grob, *Helv. Chim. Acta*, *48*, 136 (1965).
39. J. D. Schieke and V. Pretorius, *J. Chromatogr.*, *132*, 217–236 (1977).
40. C. Vidal-Madjar, J. Ganansia, and G. Guiochon, in *Gas Chromatography 1970* (R. Stock, ed.), Institute of Petroleum, London, 1971, p. 20.
41. C. Vidal-Madjar, S. Bekassy, M. F. Gonnord, P. Arpino, and G. Guiochon, *Anal. Chem.*, *49*, 768 (1977).
42. J. E. Sternberg, *Adv. Chromatogr.*, *2*, 205 (1966).
43. S. T. Sie and J. P. A. Bleumer, Unpublished Results.
44. E. van Andel, H. Kramers, and H. de Voogd, *Chem. Eng. Sci.*, *19*, 77 (1964).
45. R. N. Trivedi and K. Vasudeva, *Ibid.*, *30*, 317 (1975).
46. E. Grushka and E. J. Kikta, Jr., *J. Phys. Chem.*, *78*, 2297 (1974); *79*, 2199 (1975).
47. A. C. Ouano, *Ind. Eng. Chem. Fundam.*, *11*, 268 (1972).
48. A. C. Ouano and J. A. Carothers, *J. Phys. Chem.*, *79*, 1314 (1975).
49. R. Tijssen, *Can. J. Chem. Eng.*, *55*, 225 (1977).
50. J. F. M. Kolk, Ph.D. Dissertation, Amsterdam 1977; J. A. Moulijn, R. Spijker, and J. F. M. Kolk, *J. Chromatogr.*, *142*, 155 (1977).
51. A. B. Littlewood, *Gas Chromatography*, 2nd ed., Academic, New York, 1970.
52. D. H. Desty and A. Goldup, in *Gas Chromatography 1960* (R. P. W. Scott, ed.), Butterworths, London, 1960, p. 162.
53. G. S. F. Hazeldean and R. P. W. Scott, *Ibid.*, p. 144.
54. F. Doue and G. Guiochon, *Sep. Sci.*, *5*, 197 (1970).
55. L. F. Flint and P. Eisenklam, *Can. J. Chem. Eng.*, *47*, 101 (1969).
56. J. D. Schieke, T. W. Smuts, and V. Pretorius, *Sep. Sci.*, *3*, 27 (1968).
57. J. C. Kraak, Ph.D. Dissertation, Amsterdam, 1974.
58. M. Mohnke and W. Saffert, in *Gas Chromatography 1962* (M. van Swaay, ed.), Butterworths, London, 1962.
59. G. J. Taylor, *Proc. R. Soc. (London)*, *A225*, 473 (1954).
60. M. Novotny et al., *Anal. Chem.*, *50*, 271, 632 (1978).

Received by editor January 3, 1978